



Synthesis of PtCo₃ polyhedral nanoparticles and evolution to Pt₃Co nanoframes



Nigel Becknell^a, Cindy Zheng^a, Chen Chen^{a,b,1}, Yi Yu^a, Peidong Yang^{a,b,c,*}

^a Department of Chemistry, University of California, Berkeley, Berkeley, CA 94720, USA

^b Materials Sciences Division, Lawrence Berkeley National Laboratory, 1 Cyclotron Road, Berkeley, CA 94720, USA

^c Kavli Energy Nanoscience Institute, Berkeley, CA 94720, USA

ARTICLE INFO

Available online 8 October 2015

Keywords:

Platinum

Cobalt

Bimetallic

Nanoframe

ABSTRACT

Bimetallic nanoframes have great potential for achieving new levels of catalytic activity in various heterogeneous reactions due to their high surface area dispersion of expensive noble metals on the exterior and interior surfaces of the structure. PtCo₃ nanoparticles with polyhedral shapes were synthesized by a hot-injection method. Scanning transmission electron microscopy combined with energy dispersive X-ray spectroscopy (EDS) showed that these nanoparticles demonstrated elemental segregation of platinum to the edges of the polyhedron, forming the basis for a framework nanostructure. The process of preferential oxidative leaching which removed cobalt from the interior of the framework was tracked by EDS and inductively coupled plasma optical emission spectroscopy. This evolution procedure left the platinum-rich edges intact to form a Pt₃Co nanoframe. This is the first reported synthesis of a platinum–cobalt nanoframe and could have potential applications in catalytic reactions such as oxygen reduction.

© 2015 Elsevier B.V. All rights reserved.

1. Introduction

The importance of nanocrystal synthesis has been emphasized by the applications of nanocrystals in a vast array of fields including catalysis [1, 2], semiconductors [3], electronics [4], plasmonics [5], and magnetism [6, 7]. The nature of nano-sized metallic or semiconducting materials affords them unique and beneficial properties compared to their bulk counterparts. The ability to control the shape and structure of nanoparticles (NPs) can greatly enhance and clarify structure-dependent trends in their properties [8–10]; when two or more metals are incorporated into a single particle, the possibilities for structural control of the particle expand significantly. Bimetallic NPs have been synthesized with various geometries including core–shell [11], random distribution, and heterogeneous distribution [12]. By incorporating two metals into a nanoparticle, the capabilities of the nanoparticle can be diversified due to the synergistic interactions between the two different metals.

Recently, Yang and co-workers have employed both homogeneous and heterogeneous distributions of elements in bimetallic particles to achieve significant enhancements in catalytic activity for electrochemical carbon dioxide reduction [13] and oxygen reduction [14]. In the latter case, a PtNi₃ rhombic dodecahedron was synthesized with heterogeneous distribution of platinum to the edges of the three-dimensional shape. Nickel was then preferentially oxidized from the

faces and interior of the polyhedron, leaving a hollow nanoframe (NF) with three-dimensional catalytically active surfaces on the interior and exterior of the frame. This work demonstrated a novel method for obtaining a NF by synthesizing a bimetallic NP with heterogeneous distribution of the two elements. This method enables the synthesis of an alloy which can convert from Pt-poor to Pt-rich composition while maintaining the rigid structure of the edges of the shape. Previous work on hollow NF structures involved galvanic replacement of a template nanostructure with a more noble metal [15–18], sequential growth of metal on the edges of a template shape [19], or direct solvothermal synthesis of a hollow NF [20,21]. More recently, additional work has been done on the synthesis of bimetallic NPs with heterogeneous distribution of a noble metal to the edges of the shape [22–25]. However, to this point, no work has been reported on the synthesis of platinum–cobalt bimetallic NFs.

Platinum–cobalt bimetallic alloys have been extensively studied for their magnetic properties [26,27] and enhanced catalytic activity for the oxygen reduction reaction (ORR) [28–35]. The Pt₃Co phase was synthesized with high monodispersity by reduction of platinum acetylacetonate with concomitant decomposition of cobalt carbonyl [26,29]. Ordered PtCo NPs have been synthesized by solution-phase methods, which typically result in a disordered face centered cubic structure, and subsequent high temperature annealing to produce the ordered tetragonal PtCo phase [36]. There are very few reports of solution phase synthesis of PtCo₃ NPs [37]. In fact, the platinum–cobalt phase diagram is still in debate, with some suggesting a PtCo₃ ordered phase should be possible [38], similar to PtNi₃, and others asserting that it is not a stable

* Corresponding author.

E-mail address: p_yang@berkeley.edu (P. Yang).

¹ Department of Chemistry, Tsinghua University, Beijing 100084, PR China.

phase and that the solid solution composition of 75% cobalt is similarly unfavorable [39]. This is understandable considering that at temperatures below 450 °C, cobalt prefers its epsilon hexagonally close-packed phase [40]. It is well known that platinum strongly prefers cubic close-packing structure, so cobalt-rich platinum alloys are naturally difficult to stabilize and the more stable PtCo or Pt₃Co phases are typically preferred. We developed the synthesis of a cobalt-rich Pt–Co polyhedron because the NP must be cobalt-rich in order to make a sufficiently hollow NF by leaching of the Co. Through this synthesis and evolution process, we report the first synthesis of a Pt-rich, platinum–cobalt alloy nanoframe.

2. Experimental

2.1. PtCo₃ nanoparticle synthesis

Chloroplatinic acid hexahydrate (H₂PtCl₆·6H₂O), cobalt acetate tetrahydrate ((CH₃COO)₂Co·4H₂O), oleylamine (technical grade, 70%) and oleic acid (technical grade, 90%) were purchased from Sigma Aldrich. Chloroplatinic acid (28.5 mg) and cobalt acetate tetrahydrate (60 mg) were dissolved into 285 μL ultrapure water and then mixed with 3 mL oleylamine. This mixture was homogenized by stirring at 60 °C under nitrogen for 30 min. Oleylamine (5 mL) and oleic acid (2 mL) were added to a 25 mL three-neck flask and heated at 180 °C under argon for 45 min. Next, the precursor mixture was injected into the three-neck flask and heated under argon flow for 3 min. Then, the temperature of the reaction solution was increased to 240 °C. The solution went from dark purple to black. The NP solution was held at 240 °C for 2 min for growth of the particles before being rapidly cooled in a water bath. The particles were washed once with ethanol and a second time with hexanes and ethanol by centrifuging at 12,000 rpm for 10 min. After washing, the particles could be dispersed in solvents such as hexanes or chloroform.

2.2. Evolution to Pt₃Co nanoframes

The as-synthesized NPs (~2 mg) were dispersed into 2.5 mL chloroform with 300 μL oleylamine added. This solution was then diluted with 10 mL hexadecane and sonicated for 1 h. The suspension of NPs was then heated at 130 °C with occasional sonication required to re-disperse the highly magnetic NPs. After heating for 6 h, the NPs had fully evolved to hollow NFs.

2.3. Characterization of Pt–Co nanoparticles and nanoframes

Nanoparticle and nanoframe samples were imaged by transmission electron microscopy (TEM) using a Hitachi H-7650 TEM and scanning electron microscopy (SEM) using a Zeiss Gemini Ultra-55 Field Emission SEM to determine size and morphology. Energy dispersive spectroscopy (EDS) was also performed with TEM to determine composition of the bimetallic NPs and NFs. High resolution TEM (HRTEM) was performed with an F20 UT Tecnai to confirm crystallinity and structure of the Pt–Co samples. High-angle annular dark-field scanning transmission electron microscopy (HAADF-STEM) and EDS mapping were performed with an FEI TitanX to characterize the elemental distribution in the NPs and NFs.

The crystalline phase of the samples was determined through X-ray diffraction (XRD) with a Bruker D-8 General Area Detector Diffraction System (GADDS) with HI-STAR area CCD detector. The instrument was equipped with a Co–Kα source ($\lambda = 1.789 \text{ \AA}$). The composition of the samples was determined through XRD, EDS, and inductively coupled plasma optical emission spectroscopy (ICP-OES) using a PerkinElmer Optima 7000 DV.

The behavior of the surface of the NPs was analyzed with ambient pressure X-ray photoelectron spectroscopy (AP-XPS) on the Scienta R4000 HiPP endstation at the Lawrence Berkeley National Laboratory Advanced Light Source (ALS) Beamline 9.3.2. Samples were prepared on silicon substrates and mounted on a ceramic button heater sample holder in order to heat the sample up to 120 °C during experiments. The atmosphere was controlled at UHV ($\sim 10^{-9}$ Torr) or 100 mTorr of H₂ or O₂ by introducing the gases into the chamber through different molecular leak valves. XPS spectra were collected using an incident X-ray energy of 490 eV. The binding energy for XPS spectra was calibrated to the Au 4f core level of a Au foil. The XPS spectra were quantitatively analyzed by subtracting a Shirley background.

3. Results and discussion

3.1. PtCo₃ nanoparticle synthesis

PtCo₃ NPs were synthesized by hot-injection of Pt and Co precursors into a mixture of oleylamine and oleic acid. A typical TEM image of the as-synthesized PtCo₃ polyhedral NP is shown in Fig. 1a. The size distribution of the PtCo₃ NP was calculated to be 17.1 ± 2.7 nm. The hexagonal projection, characteristic of a rhombic dodecahedron in the

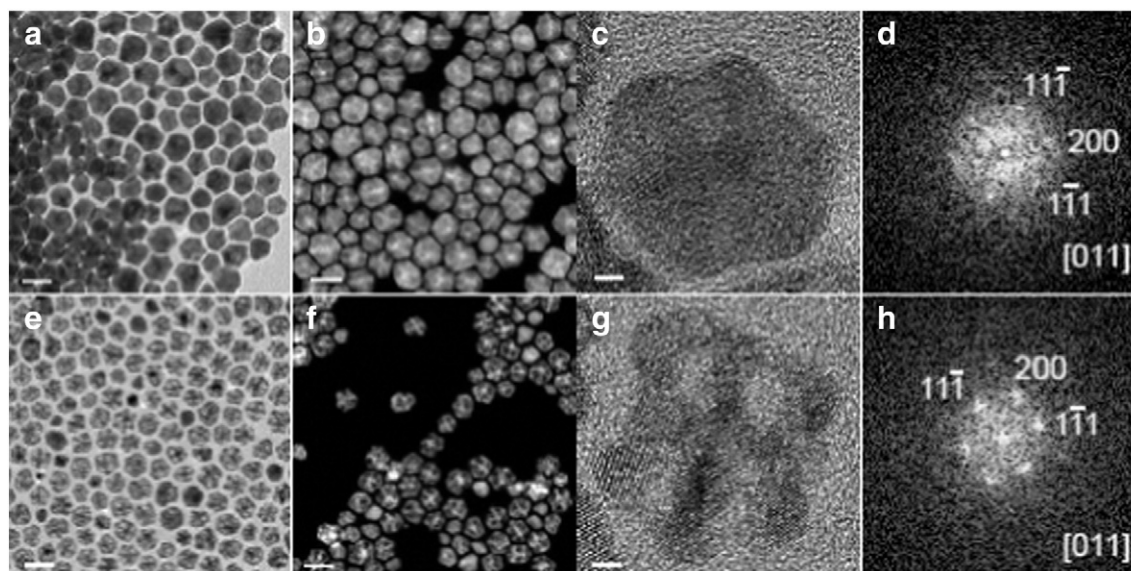


Fig. 1. (a) TEM image of PtCo₃ NP. (b) STEM image of PtCo₃ NP. (c) HRTEM image of a PtCo₃ NP and (d) corresponding FFT. (e) TEM image of Pt₃Co NF. (f) STEM image of Pt₃Co NF. (g) HRTEM image of Pt₃Co NF and (h) corresponding FFT. Scale bars in TEM/STEM images are 20 nm. Scale bars in HRTEM images are 2 nm.

platinum bimetallic, oleylamine-based system, was primarily observed in TEM though there are other polyhedra which form during the synthesis of the PtCo_3 NPs. HAADF-STEM imaging was used to screen PtCo_3 NPs for the required heterogeneous elemental distribution because it provides significant contrast difference between atoms of different atomic number [41]. The STEM image of the as-synthesized PtCo_3 polyhedra in Fig. 1b demonstrates initial proof of segregation of the heavier element, Pt, to the edges of the three-dimensional shape due to the bright contrast which can be seen at the edges.

A few key aspects of the synthesis enabled it to produce these Co-rich polyhedra. A molar ratio of 4.4:1 Co:Pt (in excess of the 3:1 ratio in the product) was required to accelerate reduction of Co^{2+} due to its more negative reduction potential compared to that of Pt^{4+} [42]. In addition, oleylamine acted as a solvent, reducing agent, and surfactant [43, 44], while oleic acid also aided as a surfactant. Oleic acid was introduced into the synthesis to enhance the shape control as it has been shown that oleic acid has a particularly strong affinity for cobalt in many cobalt-based NP syntheses [7,45–49]. Oleic acid has also been found to improve the effectiveness of oleylamine [49] and their synergistic effect was expected based on the slight temperature increase of their solution upon simple mixing of the two surfactants. Without the presence of the oleic acid, the NPs synthesized were significantly more rounded and the size was only 11.9 ± 1.6 nm (see Supplementary data Fig. S1). This result indicates oleic acid played a key role in stabilizing larger nuclei and sharpening the edges of the polyhedra during the synthesis, a critical point for transformation into the desired hollow NF. These polyhedral shapes were also observed under SEM imaging to confirm their three-dimensional structure (see Supplementary data Fig. S2).

3.2. Evolution from PtCo_3 NP to Pt_3Co NF

In order to evolve the PtCo_3 NP to a Pt_3Co NF, the NPs were dispersed in excess oleylamine and hexadecane and heated at 130°C under air atmosphere. While sufficiently stabilized by both oleylamine and oleic acid, the NPs are magnetic and do aggregate over a short period of time after washing. During the initial period of heating, the magnetic NPs continued to settle out, requiring intermediate periods of sonication to re-disperse the particles. However, once a sufficient amount of cobalt was removed, the magnetic moment of the particle could no longer be

sustained, so aggregation was not severe and sonication was no longer required. TEM and STEM images of the final evolved Pt_3Co NFs are shown in Fig. 1e and f. The hollow interior of the polyhedral frame can be seen in bright-field and dark-field images. Compared to the NPs, STEM imaging revealed more uniform intensity, or less contrast, over the area of the NFs, indicating more uniform distribution of Pt and Co.

3.3. Structural characterization of PtCo_3 NP and Pt_3Co NF

HRTEM (Fig. 1c, d, g, h) imaging and XRD (Fig. 2) indicated that the NPs and NFs had the expected face-centered cubic structure. In the XRD, the peaks corresponded well with PtCo_3 for the NP and Pt_3Co for the NF. These compositions were further supported by EDS and ICP measurements. The NP was determined to be 75% Co and the NF was 25% Co by both ICP and EDS. However, the PtCo_3 NP diffraction pattern exhibited asymmetric broadening toward the lower 2θ side, indicating the possible formation of other Pt–Co alloys. This is expected according to the known phase stability [39], which favors phase separation to the PtCo composition. Many previous reports illustrate the relatively facile synthesis of Pt_3Co or PtCo phases [26,36]. Additionally, a face-centered cubic platinum–cobalt solid solution NP was synthesized with a composition of $\text{Co}_{69}\text{Pt}_{31}$ and while more Pt-rich compositions were demonstrated, increased cobalt content was not [44]. Even impregnation and high-temperature annealing methods do not produce pure phase PtCo_3 NP alloys, but rather a mixture of two or more Pt–Co phases with an average composition of 75% Co and 25% Pt [33,50–52]. For example, Strasser et al. reported via Rietveld analysis that their PtCo_3 sample actually consisted of 74.8 ± 2.2 wt.% $\text{Pt}_{47}\text{Co}_{53}$ and 25.2 ± 2.1 wt.% $\text{Pt}_5\text{Co}_{95}$ [50], consistent with the Pt–Co phase diagram reported by Okamoto [39]. We also observed some Pt-rich NP impurities. Fig. 1f shows that some solid spherical particles remained in the NF sample and these particles exhibit little contrast in the HAADF image, indicating that they were platinum-rich impurity particles in the initial PtCo_3 NP synthesis. The diffraction pattern for the NF sample consists of symmetric peaks with significantly less broadening than that observed in the NP XRD pattern. Therefore, after evolution, the sample consists of homogeneous Pt_3Co NFs with some spherical impurities which were likely synthesized as Pt_3Co initially.

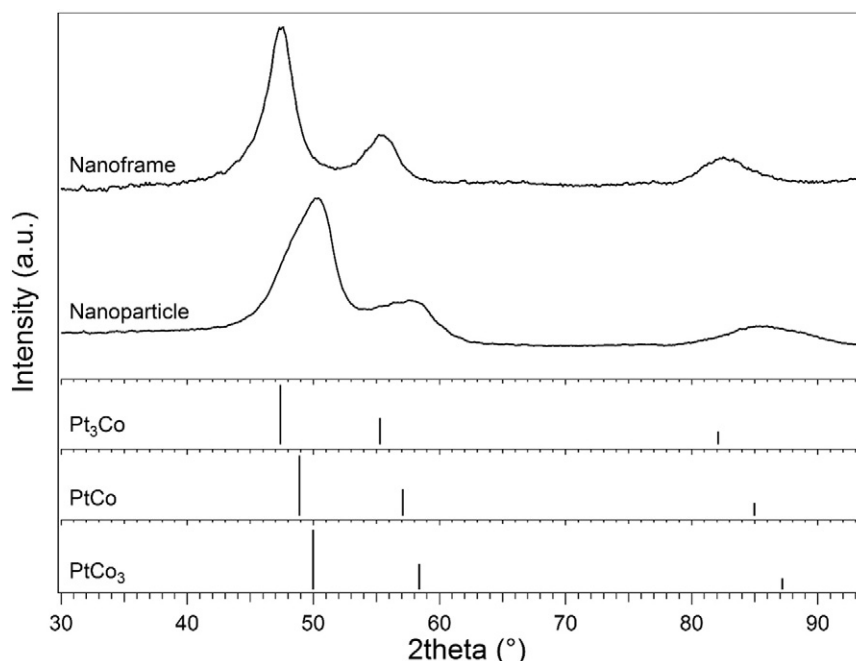


Fig. 2. XRD patterns of PtCo_3 NP and Pt_3Co NF. Diffraction patterns for Pt_3Co (JCPDS 01-072-9178), PtCo (03-065-8970), and PtCo_3 (01-071-7411) are shown for comparison.

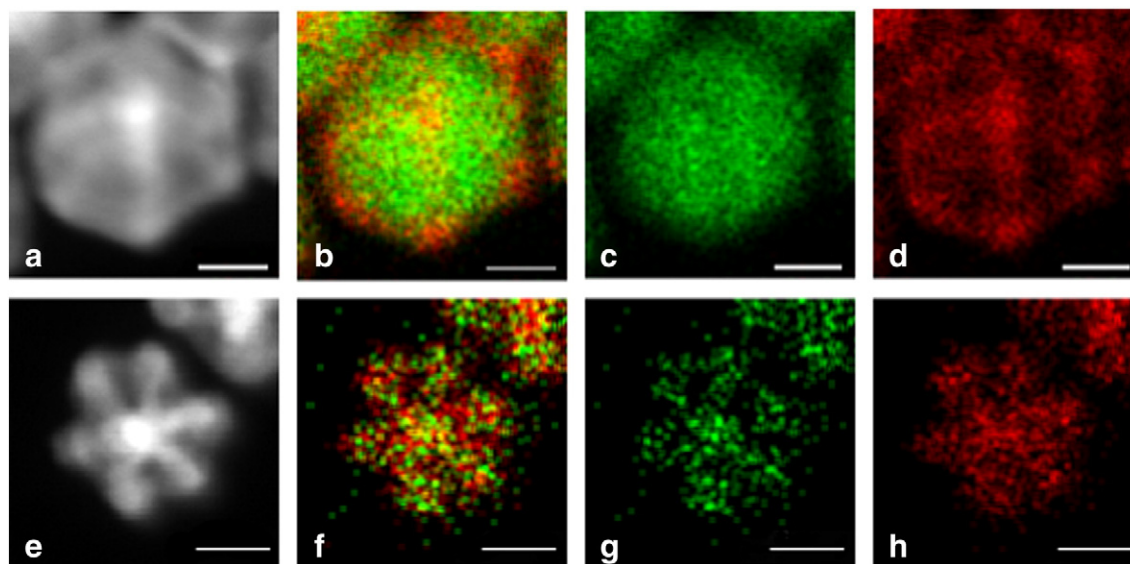


Fig. 3. (a) HAADF-STEM image of PtCo_3 NP and (b) corresponding EDS elemental mapping with separate maps shown for (c) Co and (d) Pt. (e) HAADF-STEM image of Pt_3Co NF and (f) corresponding EDS elemental mapping with separate maps shown for (g) Co and (h) Pt. All scale bars are 6 nm.

3.4. Compositional characterization of PtCo_3 NP and Pt_3Co NF

HAADF-STEM imaging and corresponding EDS mapping in Fig. 3a–d further prove that the PtCo_3 polyhedral NPs were synthesized with platinum enrichment on the edges. In the PtCo_3 NP, the edges exhibit brighter contrast (Fig. 3a) due to the enrichment of the heavier element, platinum. This is corroborated by elemental mapping which shows a cobalt-rich core (Fig. 3c) and a platinum framework (Fig. 3d) which has formed in the as-synthesized NP. Evolution of this NP yields a NF in which the HAADF imaging contrast is more uniform (Fig. 3e) and the elemental mapping demonstrates homogeneous distribution of the elements (Fig. 3f–h). The composition of the NPs could also be tracked during the evolution process via quantitative EDS (Fig. 4). The measured EDS composition matched well with the XRD and ICP-OES results in that the NP began with a composition of 75% Co, but leaching of the cobalt from the particle during solution-phase oxidation led to a NF with 25% Co composition.

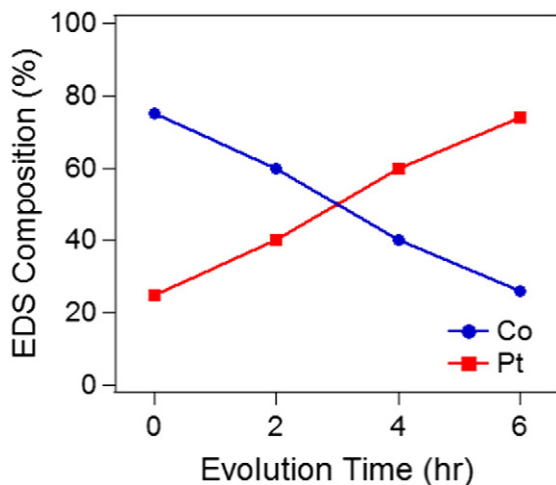


Fig. 4. Compositional evolution from PtCo_3 NP to Pt_3Co NF at 130 °C as tracked by EDS.

3.5. AP-XPS of PtCo_3 NP in different atmospheres

Further proof of the favorable oxidative leaching process was obtained through AP-XPS experiments at the ALS Beamline 9.3.2. Although XPS is a difficult method for achieving accurate quantification, the general trends of surface composition can be elucidated. The incident photon energy was tuned to 490 eV, corresponding to an inelastic mean free path of approximately 0.9 nm [53]. The changes in surface composition of the PtCo_3 NP due to different environments in the XPS chamber are shown in Fig. 5. A sample background-subtracted XPS spectrum is shown in Fig. S3. Initially, it was found that the surface of the PtCo_3 NPs may have been slightly enriched in Pt. Annealing of the NP in 100 mTorr H_2 at 120 °C only furthered this enrichment of Pt at the surface. Subsequent annealing in 100 mTorr O_2 at 120 °C produced a drastic increase in the concentration of Co at the surface of the NP. A similar increase in surface Ni concentration under O_2 was observed in the corresponding PtNi_3 nanoparticle [14]. A final annealing step in H_2 served to

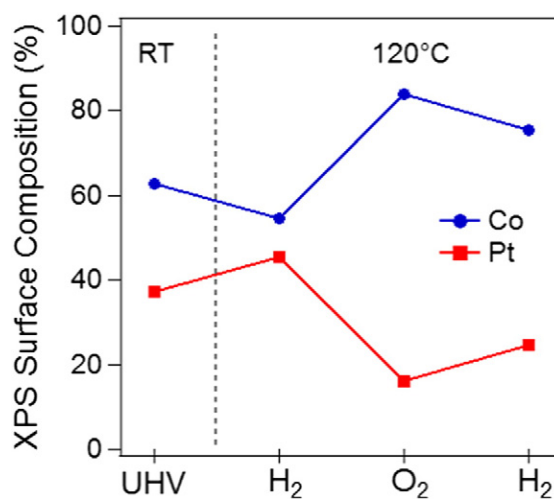


Fig. 5. AP-XPS quantitative analysis of surface composition. Initial spectrum was taken at approximately 10^{-9} Torr (UHV) at room temperature (RT). Subsequent annealing was performed in 100 mTorr of H_2 or O_2 while the sample was heated at 120 °C.

once again induce surface segregation of Pt in the PtCo₃ NP. These results demonstrate the ability of cobalt to surface segregate and be oxidized under an air atmosphere at moderately high temperature in these NPs. Therefore, the removal of cobalt from the PtCo₃ NP and evolution to the hollow Pt₃Co NF was able to proceed quite easily and over a short period of time.

4. Conclusion

PtCo₃ NPs with segregation of platinum to the edges of their polyhedral shape were synthesized by co-reduction of platinum and cobalt precursor salts. Shape control was achieved by utilizing a dual surfactant system of oleylamine and oleic acid. Due to the heterogeneous distribution of the elements in the polyhedron, cobalt was able to easily oxidize as shown in AP-XPS experiments. This allowed for leaching of cobalt from the NP and evolution to a hollow NF by solution-phase oxidation. The hollow Pt₃Co NF is the first platinum–cobalt alloy nanoframe and could have important applications in areas such as catalysis. Specifically, the alloy composition and framework structure could potentially provide excellent oxygen reduction reaction activity which is currently under investigation.

Acknowledgments

This research was supported by the Office of Science, Office of Basic Energy Sciences, of the U.S. Department of Energy under contract no. DE-AC02-05CH11231. We would like to thank Professor Paul Alivisatos for access to the Bruker D-8 XRD, the Molecular Foundry at Lawrence Berkeley National Laboratory for access to the Zeiss SEM and electron microscopes at the National Center for Electron Microscopy, Dohyung Kim for assistance with SEM imaging, Ethan Crumlin for assistance at ALS Beamline 9.3.2, and Elena Kreimer of the Microanalytical Facility in the College of Chemistry, UC Berkeley for access to ICP. The Advanced Light Source is supported by the Director, Office of Science, Office of Basic Energy Sciences, of the U.S. Department of Energy under contract no. DE-AC02-05CH11231. Work at the Molecular Foundry was supported by the Office of Science, Office of Basic Energy Sciences, of the U.S. Department of Energy under contract no. DE-AC02-05CH11231.

Appendix A. Supplementary data

Supplementary data to this article can be found online at <http://dx.doi.org/10.1016/j.susc.2015.09.024>.

References

- [1] G.A. Somorjai, J.Y. Park, *Top. Catal.* 49 (2008) 126.
- [2] A.T. Bell, *Science* 299 (2003) 1688.
- [3] Y. Yin, A.P. Alivisatos, *Nature* 437 (2005) 664.
- [4] D.V. Talapin, J.-S. Lee, M.V. Kovalenko, E.V. Shevchenko, *Chem. Rev.* 110 (2009) 389.
- [5] A. Tao, P. Sinsermsuksakul, P. Yang, *Nat. Nanotechnol.* 2 (2007) 435.
- [6] S.H. Sun, C.B. Murray, D. Weller, L. Folks, A. Moser, *Science* 287 (2000) 1989.
- [7] C.B. Murray, S.H. Sun, H. Doyle, T. Betley, *MRS Bull.* 26 (2001) 985.

- [8] K.M. Bratlie, H. Lee, K. Komvopoulos, P. Yang, G.A. Somorjai, *Nano Lett.* 7 (2007) 3097.
- [9] H. Song, F. Kim, S. Connor, G.A. Somorjai, P. Yang, *J. Phys. Chem. B* 109 (2005) 188.
- [10] Y. Yin, R.M. Rioux, C.K. Erdonmez, S. Hughes, G.A. Somorjai, A.P. Alivisatos, *Science* 304 (2004) 711.
- [11] S.E. Habas, H. Lee, V. Radmilovic, G.A. Somorjai, P. Yang, *Nat. Mater.* 6 (2007) 692.
- [12] N. Toshima, T. Yonezawa, *New J. Chem.* 22 (1998) 1179.
- [13] D. Kim, J. Resasco, Y. Yu, A.M. Asiri, P. Yang, *Nat. Commun.* 5 (2014).
- [14] C. Chen, Y. Kang, Z. Huo, Z. Zhu, W. Huang, H.L. Xin, J.D. Snyder, D. Li, J.A. Herron, M. Mavrikakis, M. Chi, K.L. More, Y. Li, N.M. Marković, G.A. Somorjai, P. Yang, V.R. Stamenkovic, *Science* 343 (2014) 1339.
- [15] G.S. Metraux, Y.C. Cao, R.C. Jin, C.A. Mirkin, *Nano Lett.* 3 (2003) 519.
- [16] X.M. Lu, L. Au, J. McLellan, Z.Y. Li, M. Marquez, Y.N. Xia, *Nano Lett.* 7 (2007) 1764.
- [17] X. Hong, D.S. Wang, S.F. Cai, H.P. Rong, Y.D. Li, *J. Am. Chem. Soc.* 134 (2012) 18165.
- [18] M.A. Mahmoud, M.A. El-Sayed, *J. Am. Chem. Soc.* 132 (2010) 12704.
- [19] S.F. Xie, N. Lu, Z.X. Xie, J.G. Wang, M.J. Kim, Y.N. Xia, *Angew. Chem. Int. Ed.* 51 (2012) 10266.
- [20] B.Y. Xia, H.B. Wu, X. Wang, X.W. Lou, *J. Am. Chem. Soc.* 134 (2012) 13934.
- [21] F. Noshien, Z.C. Zhang, J. Zhuang, X. Wang, *Nanoscale* 5 (2013) 3660.
- [22] L. Han, H. Liu, P. Cui, Z. Peng, S. Zhang, J. Yang, *Sci. Rep.* 4 (2014).
- [23] Y. Wu, D. Wang, G. Zhou, R. Yu, C. Chen, Y. Li, *J. Am. Chem. Soc.* 136 (2014) 11594.
- [24] A. Oh, H. Baik, D.S. Choi, J.Y. Cheon, B. Kim, H. Kim, S.J. Kwon, S.H. Joo, Y. Jung, K. Lee, *ACS Nano* 9 (2015) 2856.
- [25] Y. Wang, Y. Chen, C. Nan, L. Li, D. Wang, Q. Peng, Y. Li, *Nano Res.* (2015) 1.
- [26] E.V. Shevchenko, D.V. Talapin, A.L. Rogach, A. Kornowski, M. Haase, H. Weller, *J. Am. Chem. Soc.* 124 (2002) 11480.
- [27] E.V. Shevchenko, D.V. Talapin, H. Schnablegger, A. Kornowski, Ö. Festin, P. Svedlindh, M. Haase, H. Weller, *J. Am. Chem. Soc.* 125 (2003) 9090.
- [28] Y. Xu, A.V. Ruban, M. Mavrikakis, *J. Am. Chem. Soc.* 126 (2004) 4717.
- [29] C. Wang, D. van der Vliet, K.C. Chang, H.D. You, D. Strmcnik, J.A. Schlueter, N.M. Markovic, V.R. Stamenkovic, *J. Phys. Chem. C* 113 (2009) 19365.
- [30] C. Wang, G.F. Wang, D. van der Vliet, K.C. Chang, N.M. Markovic, V.R. Stamenkovic, *Phys. Chem. Chem. Phys.* 12 (2010) 6933.
- [31] C. Wang, M.F. Chi, D.G. Li, D. van der Vliet, G.F. Wang, Q.Y. Lin, J.F. Mitchell, K.L. More, N.M. Markovic, V.R. Stamenkovic, *ACS Catal.* 1 (2011) 1355.
- [32] C. Wang, N.M. Markovic, V.R. Stamenkovic, *ACS Catal.* 2 (2012) 891.
- [33] H. Schulerburg, E. Muller, G. Khelashvili, T. Roser, H. Bonnemann, A. Wokaun, G.G. Scherer, *J. Phys. Chem. C* 113 (2009) 4069.
- [34] D.L. Wang, H.L.L. Xin, R. Hovden, H.S. Wang, Y.C. Yu, D.A. Muller, F.J. DiSalvo, H.D. Abruna, *Nat. Mater.* 12 (2013) 81.
- [35] J.B. Wu, A. Gross, H. Yang, *Nano Lett.* 11 (2011) 798.
- [36] V. Tzitzios, D. Niarchos, G. Margariti, J. Fidler, D. Petridis, *Nanotechnology* 16 (2005) 287.
- [37] T.O. Ely, C. Pan, C. Amiens, B. Chaudret, F. Dassenoy, P. Lecante, M.-J. Casanove, A. Mosset, M. Respaud, J.-M. Broto, *J. Phys. Chem. B* 104 (2000) 695.
- [38] J. Sanchez, J. Moran-Lopez, C. Leroux, M. Cadeville, *J. Phys. Condens. Matter* 1 (1989) 491.
- [39] H. Okamoto, *J. Phase Equilib.* 22 (2001) 591.
- [40] B. Lee, R. Alsenz, A. Ignatiev, M. Van Hove, *Phys. Rev. B* 17 (1978) 1510.
- [41] S. Pennycook, *Ultramicroscopy* 30 (1989) 58.
- [42] P. Vanysek, *Handb. Chem. Phys.* 88 (1998).
- [43] S. Mourdikoudis, L.M. Liz-Marzan, *Chem. Mater.* 25 (2013) 1465.
- [44] Y. Yu, W. Yang, X. Sun, W. Zhu, X.-Z. Li, D. Sellmyer, S. Sun, *Nano Lett.* 14 (2014) 2778.
- [45] S. Sun, C. Murray, *J. Appl. Phys.* 85 (1999) 4325.
- [46] V.F. Puentes, K.M. Krishnan, A.P. Alivisatos, *Science* 291 (2001) 2115.
- [47] J. Zhang, J.Y. Fang, *J. Am. Chem. Soc.* 131 (2009) 18543.
- [48] J.L. Zhao, M. Spasova, Z.A. Li, M. Zharnikov, *Adv. Funct. Mater.* 21 (2011) 4724.
- [49] N.S. Porter, H. Wu, Z.W. Quan, J.Y. Fang, *Acc. Chem. Res.* 46 (2013) 1867.
- [50] M. Oezaslan, F. Hasché, P. Strasser, *J. Electrochem. Soc.* 159 (2012) B394.
- [51] F. Hasché, M. Oezaslan, P. Strasser, *ChemCatChem* 3 (2011) 1805.
- [52] M. Oezaslan, P. Strasser, *J. Power Sources* 196 (2011) 5240.
- [53] C. Powell, A. Jablonski, NIST Electron Inelastic-Mean-Free-Path Database, Version 1.2, SRD 71, National Institute of Standards and Technology, Gaithersburg, MD, 2010.